

RESEARCH

Open Access



A NOTCH1/LSD1/BMP2 co-regulatory network mediated by miR-137 negatively regulates osteogenesis of human adipose-derived stem cells

Cong Fan^{1,2,3,4,5,6*} , Xiaohan Ma^{7,8}, Yuejun Wang⁷, Longwei Lv^{2,3,4,5,6,7}, Yuan Zhu⁷, Hao Liu⁹ and Yunsong Liu^{7,2,3,4,5,6}

Abstract

Background: MicroRNAs have been recognized as critical regulators for the osteoblastic lineage differentiation of human adipose-derived stem cells (hASCs). Previously, we have displayed that silencing of miR-137 enhances the osteoblastic differentiation potential of hASCs partly through the coordination of *lysine-specific histone demethylase 1* (*LSD1*), *bone morphogenetic protein 2* (*BMP2*), and *mothers against decapentaplegic homolog 4* (*SMAD4*). However, still numerous molecules involved in the osteogenic regulation of miR-137 remain unknown. This study aimed to further elucidate the epigenetic mechanisms of miR-137 on the osteogenic differentiation of hASCs.

Methods: Dual-luciferase reporter assay was performed to validate the binding to the 3' untranslated region (3' UTR) of *NOTCH1* by miR-137. To further identify the role of *NOTCH1* in miR-137-modulated osteogenesis, tangeretin (an inhibitor of *NOTCH1*) was applied to treat hASCs which were transfected with miR-137 knockdown lentiviruses, then together with negative control (NC), miR-137 overexpression and miR-137 knockdown groups, the osteogenic capacity and possible downstream signals were examined. Interrelationships between signaling pathways of *NOTCH1-hairy and enhancer of split 1* (*HES1*), *LSD1* and *BMP2-SMADs* were thoroughly investigated with separate knockdown of *NOTCH1*, *LSD1*, *BMP2*, and *HES1*.

Results: We confirmed that miR-137 directly targeted the 3' UTR of *NOTCH1* while positively regulated *HES1*. Tangeretin reversed the effects of miR-137 knockdown on osteogenic promotion and downstream genes expression. After knocking down *NOTCH1* or *BMP2* individually, we found that these two signals formed a positive feedback loop as well as activated *LSD1* and *HES1*. In addition, *LSD1* knockdown induced *NOTCH1* expression while suppressed *HES1*.

Conclusions: Collectively, we proposed a *NOTCH1/LSD1/BMP2* co-regulatory signaling network to elucidate the modulation of miR-137 on the osteoblastic differentiation of hASCs, thus providing mechanism-based rationale for miRNA-targeted therapy of bone defect.

Keywords: MicroRNA, Human adipose-derived stem cells, Osteogenesis, *NOTCH1*, Signaling

* Correspondence: congcongsherry@sina.com

¹Department of General Dentistry II, Peking University School and Hospital of Stomatology, Beijing, China

²National Center of Stomatology, Beijing, China

Full list of author information is available at the end of the article



© The Author(s). 2021 **Open Access** This article is licensed under a Creative Commons Attribution 4.0 International License, which permits use, sharing, adaptation, distribution and reproduction in any medium or format, as long as you give appropriate credit to the original author(s) and the source, provide a link to the Creative Commons licence, and indicate if changes were made. The images or other third party material in this article are included in the article's Creative Commons licence, unless indicated otherwise in a credit line to the material. If material is not included in the article's Creative Commons licence and your intended use is not permitted by statutory regulation or exceeds the permitted use, you will need to obtain permission directly from the copyright holder. To view a copy of this licence, visit <http://creativecommons.org/licenses/by/4.0/>. The Creative Commons Public Domain Dedication waiver (<http://creativecommons.org/publicdomain/zero/1.0/>) applies to the data made available in this article, unless otherwise stated in a credit line to the data.

Background

As we know, human adipose-derived stem cells (hASCs) have multilineage differentiation potentials and good application prospects for bone regeneration [1–3] because of their abundant sources and easy access for clinical uses [4]. Though plenty of signaling pathways, such as *Wnt/β-catenin* signal [5], *glycogen synthase kinase 3* signal [6], *bone morphogenetic protein (BMP)* signal [7–9], *NOTCH* signal [10, 11], and *extracellular regulated protein kinases* signal [7, 12, 13] have been demonstrated to dominate osteoblastic differentiation of hASCs, considerable research is still necessary to reveal intricate interactions between various signals and make further advances in hASC-based cell therapy.

MicroRNAs (MiRNAs) are a class of endogenous and highly conserved small non-coding single-stranded RNAs, which mediate post-transcriptional gene regulation [14] and play crucial roles in the proliferation and osteogenic differentiation of hASCs [5, 10, 15–18]. MiR-137 has manifested its anti-tumor activity in multiple malignancies, such as glioblastoma [19], melanoma [20], multiple myeloma [21], non-small cell lung cancer [22], and endometrial cancer [23]. In neural development, several studies confirm that miR-137 regulates cell proliferation, differentiation [24–28], and neuronal maturation [29–31] in adult or mouse stem cells. Nevertheless, during the process of hASCs differentiating into osteoblastic lineage, the function and epigenetic mechanisms of miR-137 have not been investigated except for our previous study [32], in which we disclose part of the mechanisms as the coordination between *lysine-specific histone demethylase 1 (LSD1)* and *BMP2-mothers against decapentaplegic homolog 4 (SMAD4)* pathway. Considering that the relationships of osteogenesis-associated signals are complex and diverse, and massive molecules participating in the *LSD1/BMP2/SMAD4* network remain unascertained, we need to further clarify the regulatory mechanisms of miR-137 on the osteogenesis.

NOTCH signal is a fundamental pathway in bone remodeling and skeletal homeostasis [33–35]. *Hairy and enhancer of split 1 (HES1)*, a downstream gene of *NOTCH* [36], is responsible for the actions of *NOTCH* in the skeleton, even though its osteogenic effects are cell type-specific and context-dependent. By interacting with *runt-related transcription factor 2 (RUNX2)*, *HES1* induces *osteopontin* promoter [37]. But *HES1* also binds to the *osteocalcin (OCN)* promoter and suppresses its transcription in osteoblastic cells [38]. *HES1* inactivation not only increases the femoral length and trabecular number in the limb bud of transgenic mice, but also enhances mineral apposition rate and suppresses bone resorption [39]. *NOTCH1* has emerged as a target of miR-137 in human renal mesangial cells [40], retinal ganglion cells [41], neurons [42], non-small cell lung cancer cells

[43], and breast cancer cells [44], but whether it is directly inhibited by miR-137 has not yet been identified in hASCs. In small cell lung cancer cells, *NOTCH1* pathway is activated by *LSD1* inhibitor and suppressed due to the binding of *LSD1* [45]. Additionally, the induction of *NOTCH* signal impairs the activation of *BMP* pathway and the osteoblastic differentiation of dental follicle cells [46]. In contrast, *NOTCH1* upregulates *BMP2* expression in human aortic valve interstitial cells through the stimulation of *NF-κB* [47]. Our previous study confirmed that miR-137 knockdown induced *BMP2-SMAD4* pathway through the downregulation of *LSD1* dependently or independently [32], which coincides with the studies stating that *LSD1* inhibition leads to increased *BMP2* expression [48, 49]. Accordingly, we postulate a signaling network entailing *NOTCH1-HES1*, *LSD1*, and *BMP2-SMADs* pathways to unveil the miR-137 modulation on the osteogenesis of hASCs.

This study identified the interactions of miR-137 and its downstream genes and revealed that the co-regulatory signaling network of *NOTCH1/LSD1/BMP2* mediated by miR-137 negatively modulated the osteogenesis of hASCs, suggesting that miR-137 might be applied as a promising therapeutic target for bone regeneration.

Methods

Mice

The animal experiments were conducted in strict conformity with the guidelines of Animal Welfare Committee of Health Science Center in Peking University (LA2019019). Male, 5-week-old BALB/c-nu/nu nude mice (Charles River, Wilmington, MA, USA) were randomly assigned to 3 groups ($n = 6$ per group) and maintained with specific pathogen-free conditions.

Cell lines

The hASCs isolated from three separate donors were purchased in ScienCell Research Laboratories (Carlsbad, CA, USA). For each donor, the in vitro cell experiments were performed at least three times individually. For proliferation culture, cells were maintained in proliferation medium (PM), containing Dulbecco's modified Eagle's medium (Thermo Fisher Scientific, Rockford, IL, USA), 1% (v/v) penicillin/streptomycin (Thermo Fisher Scientific) and 10% (v/v) fetal bovine serum (ExCell Bio, Shanghai, China). When the cells reached 70–80% confluence, osteoinduction was performed by adding osteogenic medium (OM), which contained the above culture medium for promoting proliferation, 100 nM dexamethasone (Sigma-Aldrich), 0.2 mM L-ascorbic acid (Sigma-Aldrich), and 10 mM β-glycerophosphate (Sigma-Aldrich). The cell culture conditions were 37 °C with 5% CO₂ and 100% relative humidity.

Lentivirus transfection

Recombinant lentiviruses carrying green fluorescent protein (GFP)-tagged plasmid vectors of negative control (NC), miR-137 overexpression (miR-137), miR-137 knockdown (anti-miR-137), *NOTCH1* shRNA (anti-*NOTCH1*), *LSD1* shRNA (anti-*LSD1*), *BMP2* shRNA (anti-*BMP2*), and *HES1* shRNA (anti-*HES1*) (Additional file 5: Table S1) were produced and packaged by GenePharma (Suzhou, Jiangsu, China). Lentiviral transfection of hASCs were conducted at a multiplicity of infection of 100 for 24 h with the presence of 5 mg/mL polybrene, and then selected by 1 µg/ml puromycin (Sigma-Aldrich). The transfection rates of lentiviruses were estimated by counting the number of GFP-tagged cells and total cells with an inverted fluorescence microscope (TE2000-U, Nikon, Tokyo, Japan). The hASCs transfected with miR-137 knockdown lentiviruses were seeded in 96-well plates (1 × 10⁴ cells/well) and treated with tangeretin (an inhibitor of *NOTCH1*; APEX BIO, Houston, TX, USA) at a concentration of 5 µM before the examination of osteogenic differentiation ability and downstream gene expression.

Alkaline phosphatase (ALP) staining and quantification

After 7 days of culture in PM or OM, the hASCs were used for ALP staining and activity test according to the published protocol [10]. ALP staining was operated following the BCIP/NBT staining kit (Beyotime, Shanghai, China) instructions. For the quantitative tests of ALP activities, cells were washed with phosphate buffer saline (PBS) and 1% Triton X-100 (Solarbio, Beijing, China), then scraped in milli-Q water and subjected to three cycles of freezing and thawing. By employing the BCA method and the pierce BCA protein assay kit (Thermo Fisher Scientific), total protein was read at 562 nm and computed with a bovine serum albumin standard curve according to the manufacturer's protocol. Afterwards, ALP activity was detected at 520 nm applying an alkaline phosphatase assay kit (Jiancheng, Nanjing, Jiangsu, China) and finally normalized to the total protein concentrations of cells.

Alizarin red S (ARS) staining and quantification

After 14 days of culture in PM or OM, the hASCs were applied to detect the matrix mineralization. Following being fixed with 95% ethanol for 30 min, cells were soaked in 1% ARS staining solution (pH 4.2; Sigma-Aldrich, St. Louis, MO, USA) for 20 min at room temperature. To assess the degree of mineralization, stained areas of each well were separately dissolved in 100 mM cetylpyridinium chloride (Sigma-Aldrich) for 1 h and the absorbances were detected at 562 nm. Finally, the relative ARS intensity was normalized to the total protein concentrations of cells.

RNA extraction, reverse transcription, and quantitative real-time polymerase chain reaction (qRT-PCR)

After 3, 7, and 14 days of culture in PM or OM respectively, total RNA of cells was isolated with TRIzol (Invitrogen, Carlsbad, CA, USA) and synthesized into the first-strand cDNA using a reverse transcription system (Takara, Tokyo, Japan). All the transcripts were quantified using the FastStart universal SYBR green master (ROX) (Roche, Indianapolis, IN, USA) and a 7500 real-time PCR detection system (Applied Biosystems, Foster City, CA, USA). Relative expression levels of mRNA and miRNA were normalized to *GAPDH* mRNA and *U6* snRNA, respectively. The sequences of the primers employed are listed in Additional file 6: Table S2.

Western blotting

The hASCs were rinsed with ice PBS three times and immersed in RIPA buffer (HuaxingBio, Beijing, China) mixed with protease inhibitor cocktail (HuaxingBio). The pierce BCA protein assay kit (Thermo Fisher Scientific) was used to determine the protein concentration. A 25-µg sample of protein was added and separated by 10% sodium dodecyl sulfate-polyacrylamide gel electrophoresis, then followed by transfer to the polyvinylidene difluoride membranes (Millipore, Bedford, MA, USA). Strips on the membranes were blocked with 5% nonfat dry milk (BioRuler, Danbury, CT, USA) for 1 h at room temperature, incubated overnight at 4 °C with primary antibodies at a dilution of 1:1000, and then for 1 h at room temperature with goat anti-rabbit secondary antibodies labeled with horseradish peroxidase (ZSGB-BIO, Beijing, China; ZB-2301) at a dilution of 1:10,000. The primary antibodies used were as follows: anti-GAPDH (ZSGB-BIO; TA-08), anti-NOTCH1 (Cell Signaling Technology, Beverly, MA, USA; 3608S), anti-HES1 (Abcam, Cambridge, UK; ab108937), anti-LSD1 (Cell Signaling Technology; 2139S), anti-BMP2 (Abcam; ab14933), anti-SMAD4 (Abcam; ab40759), anti-phosphorylated SMAD1/5 (anti-p-SMAD1/5; Cell Signaling Technology; 9516S), and anti-RUNX2 (Cell Signaling Technology; 12556). Relative band intensities were measured with the ImageJ software.

Dual-luciferase reporter assay

The 3' untranslated region (3' UTR) alignments of the target regions in *NOTCH1* were predicted by TargetScan and RNA22. Reporter vectors were constructed based on the previous method [32]. The 3' UTR sequences of *NOTCH1*, which contained the possible binding sites of miR-137, were PCR amplified and then inserted into pEZX-MT06 vectors (GeneCopeia, Rockville, MD, USA) to create *NOTCH1*-WT (wild-type *NOTCH1*) luciferase reporter plasmids. Mutated forms were generated by site-directed mutagenesis (GeneCopeia) and named *NOTCH1*-MT (mutant-type *NOTCH1*) luciferase

reporter plasmids. For luciferase assay, the hASCs were planted on 24-well culture plates with a density of 5×10^4 /well and co-transfected with 1 μ g *NOTCH1*-WT or *NOTCH1*-MT plasmids, 100 nM NC or miR-137 mimics, and lipofectamine 3000 (Invitrogen). The luciferase activities were examined by a dual-luciferase reporter assay system (Promega, Madison, WI, USA) 48 h later, and standardized to renilla luciferase activity for each transfected well.

Heterotopic osteogenesis examinations *in vivo*

After the transfection with NC, miR-137 and anti-miR-137 lentiviruses, hASCs of the third passage were maintained in PM for 1 week, collected, and incubated with auto-setting calcium phosphate cement (ACPC; Rebone, Shanghai, China) for 1 h at 37 °C. Then the hASC-ACPC mixtures were transplanted subcutaneously to the dorsal regions of nude mice ($n = 6$ per group) for the analyses of heterotopic bone formation *in vivo* 8 weeks later. After being collected and fixed in 4% paraformaldehyde, the samples were photographed with soft X-ray. The radiograph was obtained by applying a Senograph 2000D molybdenum-rhodium twin target X-ray apparatus (GE, Fairfield, CT, USA). The radiation distance is 200 mm and the radiographing conditions were 22.0 kV, 35.0 mA. For histological evaluation, the specimens were decalcified in 10% ethylene diamine tetraacetic acid solution (pH 7.4) for 14 days, embedded into paraffin, then sliced into 5 μ m-thick sections before the subsequent hematoxylin and eosin (HE) staining and Masson trichrome staining. The rabbit anti-OCN primary antibodies diluted to 1:100 (Servicebio, Wuhan, Hubei, China; GB11233) were used for immunohistochemical (IHC) staining.

Statistical analysis

Data and statistical analyses were conducted with SPSS Statistics 20.0 software (IBM, Armonk, NY, USA). All data were shown as mean \pm standard deviation (SD) of three individual experiments. For the comparison of two independent or multiple groups, Mann-Whitney *U* test or Kruskal-Wallis test were applied, respectively. A two-tailed test with *p* value < 0.05 was indicated as statistically significant.

Results

MiR-137 reversely regulates hASC differentiation along osteoblastic lineage *in vitro*

Our previous study displayed an overall downward expression trend of miR-137 in hASCs during the osteoblastic induction and identified its negative role in this biological process [32]. Since lacking other studies on the osteogenic function of miR-137, we re-verified the reliability of our previous results. After transfecting

hASCs with lentiviruses of NC, miR-137 overexpression, and miR-137 knockdown (Additional file 1: Fig. S1a), we evaluated the transfection rate was over 90% by computing the percentage of GFP-tagged cells (Additional file 1: Fig. S1b). Meanwhile, the transfection effects were quantitatively determined on 3 days, 7 days, and 14 days by qRT-PCR analysis (Additional file 1: Fig. S1c).

ALP staining and activity assays displayed that miR-137 overexpression reduced ALP activity of hASCs under proliferation condition or osteogenic induction, but miR-137 knockdown reversed the effects observed with miR-137 overexpression (Additional file 2: Fig. S2a, b). ARS staining and quantification were applied to test the calcium deposits of extracellular matrix. More mineralized nodules were presented in miR-137 knockdown group while less in miR-137 overexpression group when both were compared with NC group (Additional file 2: Fig. S2c, d). Besides, the characteristic genes expressed in different stages of osteogenesis, including *RUNX2*, *ALP*, and *OCN*, were examined by qRT-PCR and presented significant decreases in miR-137 overexpression group but dramatically increased in miR-137 knockdown group (Additional file 2: Fig. S2e). According to these data, we substantiated that miR-137 inhibits *in vitro* osteoblastic activity of hASCs.

MiR-137 reversely regulates hASC differentiation along osteoblastic lineage *in vivo*

In order to validate *in vivo* osteogenic effects of miR-137, hASCs were transfected with NC, miR-137, and anti-miR-137 lentiviruses and separately mixed with ACPC, and then the compounds were subcutaneously implanted into the dorsum of nude mice (Additional file 3: Fig. S3a). After 8 weeks, the total volume and mean density of the harvested samples were assessed and manifested an apparent enhancement in miR-137 knockdown group but remarkable reduction in miR-137 overexpression group (Additional file 3: Fig. S3b, c).

Histological analyses of bone formation were performed by staining of HE, Masson trichrome, and IHC staining for OCN. HE staining showed more new bone formation in miR-137 knockdown group when comparing with NC group, which displayed only a very small amount of osteoid, but we could hardly observe any new bone or osteoid in miR-137 overexpression group. Similarly, thicker and more compact blue-green-stained collagen fiber bundles were detected in miR-137 knockdown group than in another two groups, but overexpression of miR-137 led to the thinnest collagen deposition. Moreover, we found that dark-brown stained OCN granules were the most widespread in the cells of miR-137 knockdown group, fewer in NC group, and none could be discerned in miR-137 overexpression group (Additional file 3: Fig. S3d). Consequently, in accordance with

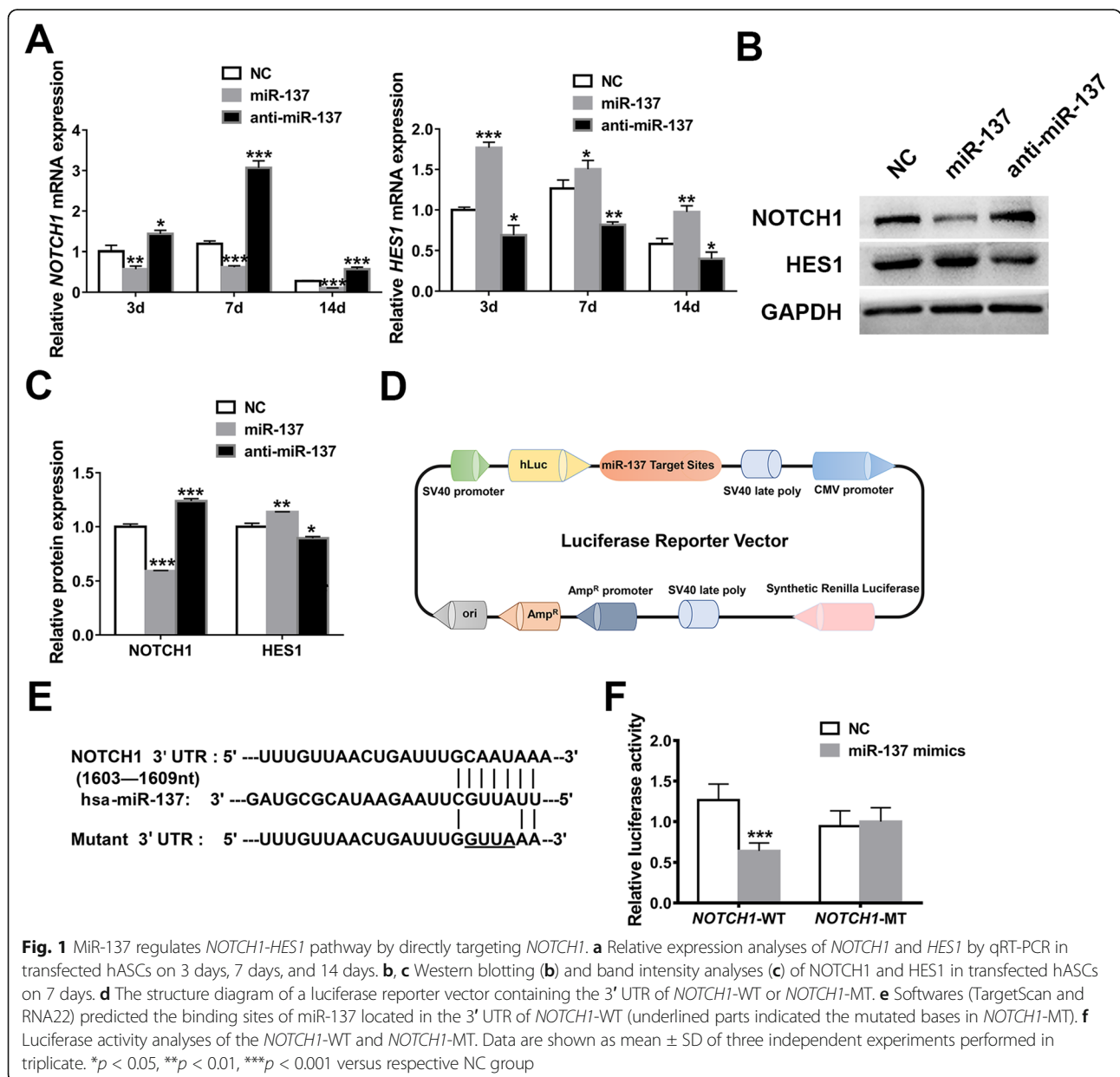
the results of in vitro experiments, miR-137 subdues the osteoblastic activity of hASCs in vivo.

MiR-137 regulates NOTCH1-HES1 pathway by directly targeting NOTCH1

To ascertain the influences of miR-137 on NOTCH1 pathway, we first examined the expression of NOTCH1 and its downstream signal HES1 with miR-137 overexpression or knockdown. When compared with NC group, the mRNA and protein levels of NOTCH1 showed obvious increase in miR-137 knockdown group while marked reduction in miR-137 overexpression group. Contrary to NOTCH1, the

expression tendency of HES1 accorded with the changes of miR-137 (Fig. 1a–c). These findings suggested that NOTCH1 is negatively regulated while HES1 is positively regulated by miR-137.

To further identify whether miR-137 could directly bind to NOTCH1 in hASCs as it does in other cell lines [40–44], dual-luciferase reporter assays were carried out. The presumed targeting sites of miR-137 in the 3' UTR of NOTCH1 were forecasted by two prediction softwares (TargetScan and RNA22). Then the luciferase reporter vectors carrying the 3' UTR of NOTCH1-WT or NOTCH1-MT were constructed (Fig. 1d, e) and the



relative luciferase activities were detected. MiR-137 mimics significantly repressed the luciferase activity in *NOTCH1*-WT group while they had no significant influences in *NOTCH1*-MT group when both groups were compared with their respective NC group (Fig. 1f). These results validated that miR-137 directly binds to the 3' UTR of *NOTCH1* and induces the expression of *HES1* in hASCs.

NOTCH1 inhibitor reverses the effects of miR-137 knockdown on osteogenesis and downstream genes expression

To confirm whether miR-137 regulated osteogenesis through *NOTCH1*, we employed *NOTCH1* inhibitor (tangeretin) in hASCs transfected with miR-137 knockdown lentiviruses. In vitro osteogenic stainings and quantification manifested that when compared with NC

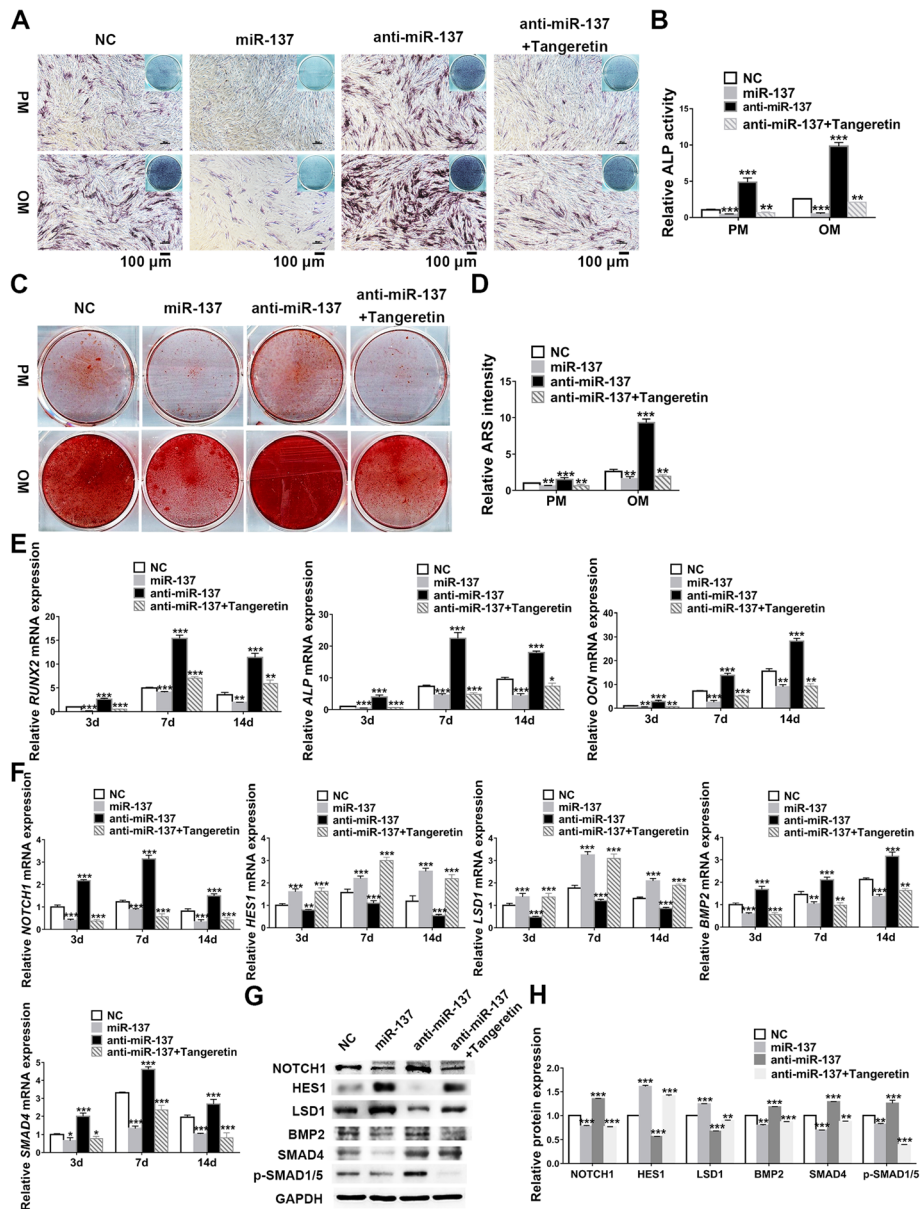


Fig. 2 *NOTCH1* inhibitor (tangeretin) reverses the effects of miR-137 knockdown on osteogenesis and downstream genes expression. **a, b** ALP staining (**a**) and quantification (**b**) of transfected hASCs after a 7-day culture in PM or OM (scale bar = 100 μm). **c, d** ARS staining (**c**) and quantification (**d**) of transfected hASCs after a 14-day culture in PM or OM. **e** Relative expression analyses of *RUNX2*, *ALP*, and *OCN* by qRT-PCR in transfected hASCs on 3 days, 7 days, and 14 days. **f** Relative expression analyses of *NOTCH1*, *HES1*, *LSD1*, *BMP2*, and *SMAD4* by qRT-PCR in transfected hASCs on 3 days, 7 days, and 14 days. **g, h** Western blotting (**g**) and band intensity analyses (**h**) of *NOTCH1*, *HES1*, *LSD1*, *BMP2*, *SMAD4*, and p-SMAD1/5 in transfected hASCs on 7 days. Data are shown as mean ± SD of three independent experiments performed in triplicate. *p < 0.05, **p < 0.01, ***p < 0.001 versus respective NC group

group, miR-137 knockdown evidently strengthened ALP activity and extracellular matrix calcification, whereas the promoted osteogenic ability caused by miR-137 knockdown were completely reversed by tangeretin treatment, and miR-137 overexpression group displayed impaired osteogenic differentiation potential as previously mentioned (Fig. 2a–d). In accord with the results of osteogenic stainings, qRT-PCR detection showed that

the expression of *RUNX2*, *ALP*, and *OCN* were enhanced in miR-137 knockdown group while reduced in miR-137 overexpression group, but the addition of tangeretin abrogated the induction of these genes by miR-137 knockdown and even suppressed their expression (Fig. 2e).

To further authenticate whether *NOTCH1* mediated the mechanisms of the osteogenic regulation by miR-

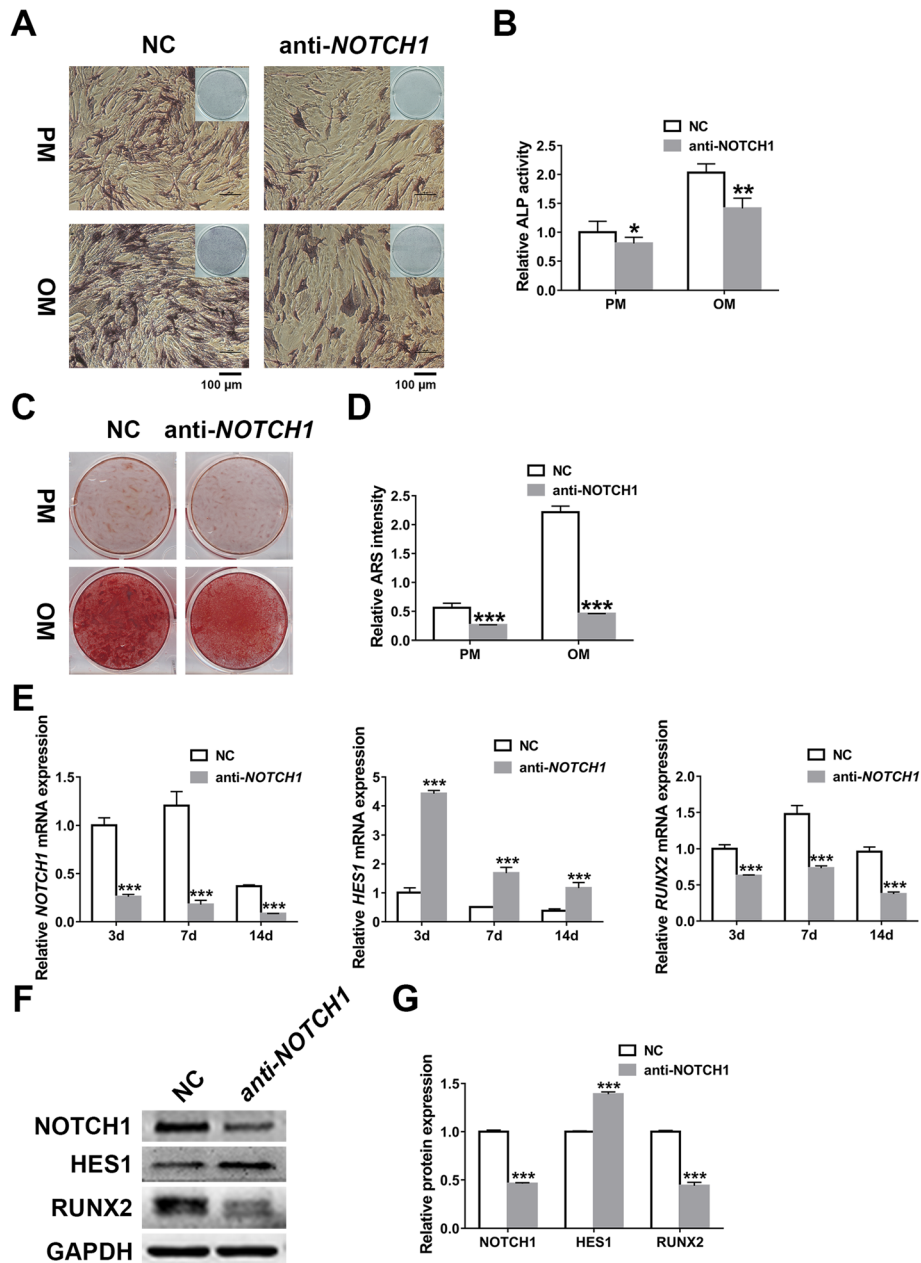


Fig. 3 *NOTCH1* knockdown impairs osteogenesis by inducing *HES1*. **a, b** ALP staining (**a**) and quantification (**b**) of transfected hASCs after a 7-day culture in PM or OM (scale bar = 100 μm). **c, d** ARS staining (**c**) and quantification (**d**) of transfected hASCs after a 14-day culture in PM or OM. **e** Relative expression analyses of *NOTCH1*, *HES1*, and *RUNX2* by qRT-PCR in transfected hASCs on 3 days, 7 days, and 14 days. **f, g** Western blotting (**f**) and band intensity analyses (**g**) of *NOTCH1*, *HES1*, and *RUNX2* in transfected hASCs on 7 days. Data are shown as mean ± SD of three independent experiments performed in triplicate. **p* < 0.05, ***p* < 0.01, ****p* < 0.001 versus respective NC group

137, we examined the expression of miR-137 downstream signals in the above four groups. Both in miR-137 overexpression and tangeretin-treated groups, *NOTCH1* was significantly repressed, though miR-137 knockdown induced its expression. The mRNA and protein expression showed that *HES1* and *LSD1* changed synchronously with the alterations of miR-137, but tangeretin-treated group inverted the downregulation of these two genes by miR-137 knockdown when compared with NC group. In addition, the mRNA or protein expression levels of *BMP2*, *SMAD4*, and p-SMAD1/5 showed that these genes were induced by miR-137 knockdown while inhibited by miR-137 overexpression. Similarly, tangeretin inhibited the activation of *BMP2*-

SMADs pathway initiated by miR-137 knockdown (Fig. 2f–h). Combined with the above results, we affirmed that *NOTCH1* inhibitor reverses the osteogenic modulation effects of miR-137 knockdown.

NOTCH1 knockdown impairs osteogenesis by inducing HES1

To determine the influences of *NOTCH1* knockdown on the osteoblastic potential of hASCs, we applied ALP and ARS stainings combined with quantitative analysis and found that *NOTCH1* knockdown attenuated ALP activity and extracellular mineralization (Fig. 3a–d). As the downstream molecules of *NOTCH1*, *HES1*, and *RUNX2* were further detected at

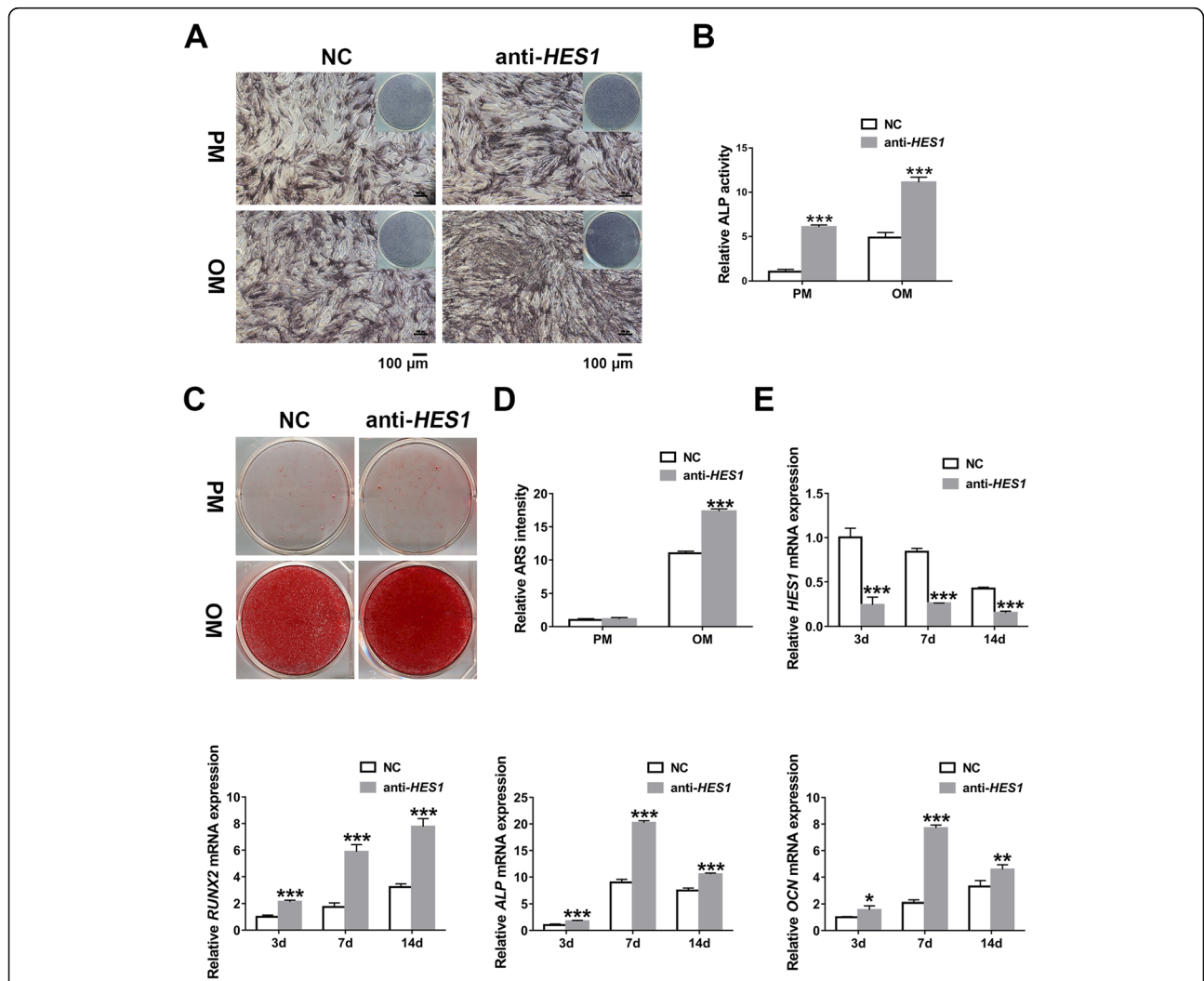


Fig. 4 *HES1* knockdown promotes osteogenesis of hASCs in vitro. **a, b** ALP staining (**a**) and quantification (**b**) of transfected hASCs after a 7-day culture in PM or OM (scale bar = 100 μm). **c, d** ARS staining (**c**) and quantification (**d**) of transfected hASCs after a 14-day culture in PM or OM. **e** Relative expression analyses of *HES1*, *RUNX2*, *ALP*, and *OCN* by qRT-PCR in transfected hASCs on 3 days, 7 days, and 14 days. Data are shown as mean ± SD of three independent experiments performed in triplicate. **p* < 0.05, ***p* < 0.01, ****p* < 0.001 versus respective NC group

mRNA and protein levels in hASCs transfected with *NOTCH1* knockdown lentiviruses. Coincident with the impacts of miR-137 on *NOTCH1-HES1* pathway, *NOTCH1* knockdown induced the expression of *HES1* while repressed *RUNX2* (Fig. 3e–g). Our results indicated that *NOTCH1* knockdown impedes the osteogenic potential of hASCs by the stimulation of *HES1*, corroborating the former conclusions that miR-137 inhibits osteogenesis by the downregulation of *NOTCH1* and upregulation of *HES1*.

Then we checked the impacts of *HES1* on the osteogenic differentiation of hASCs. After knocking down *HES1*, we examined the osteogenic ability by the application of osteogenic stainings and quantification as well as qRT-PCR detection of *RUNX2*, *ALP*, and *OCN*. All these in vitro osteogenic tests showed promoted osteogenic potential of hASCs with *HES1* knockdown (Fig. 4). Therefore, we demonstrated that *HES1* plays a negative role in the osteoblastic

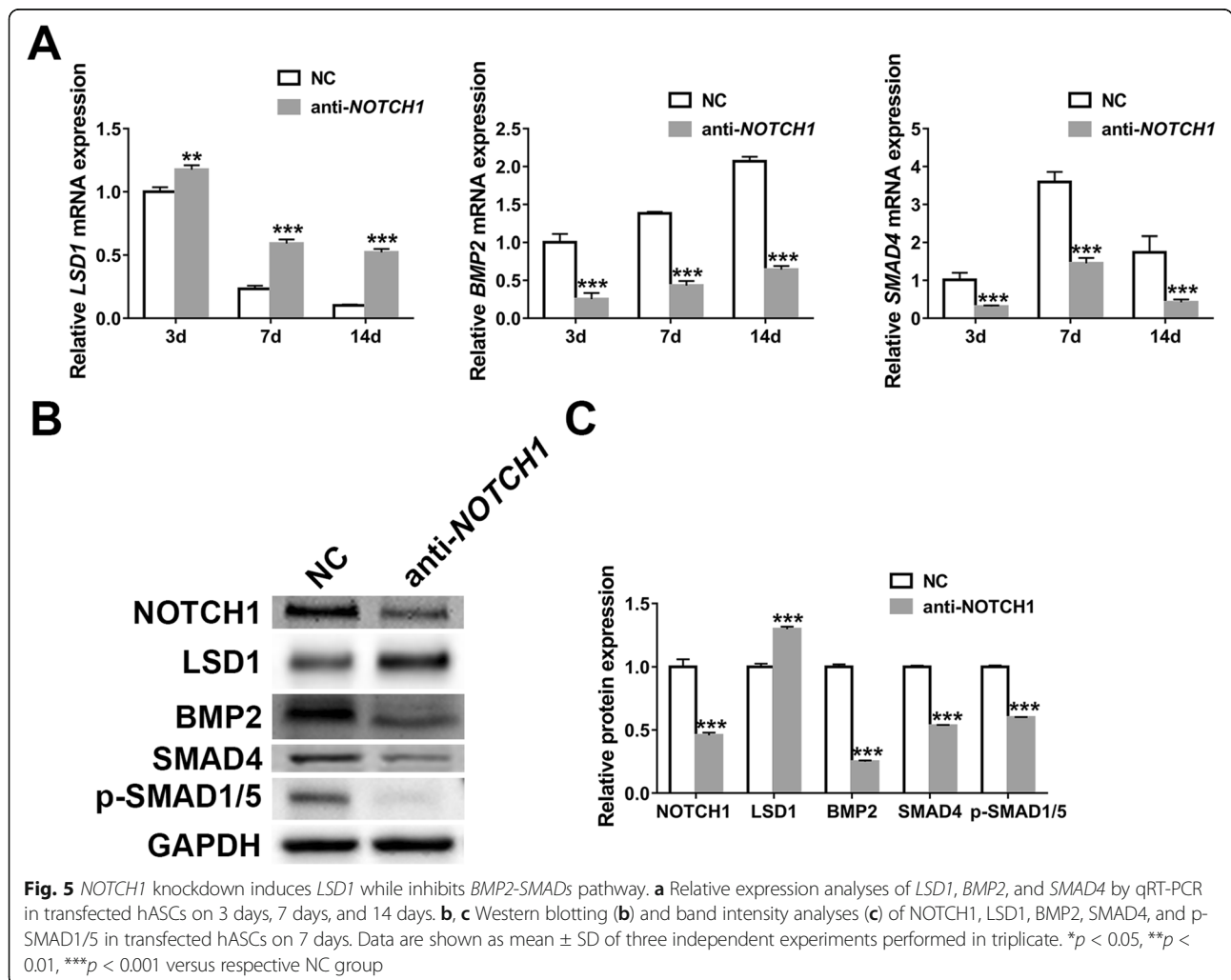
differentiation of hASCs and intervenes in *NOTCH1*-induced osteogenesis.

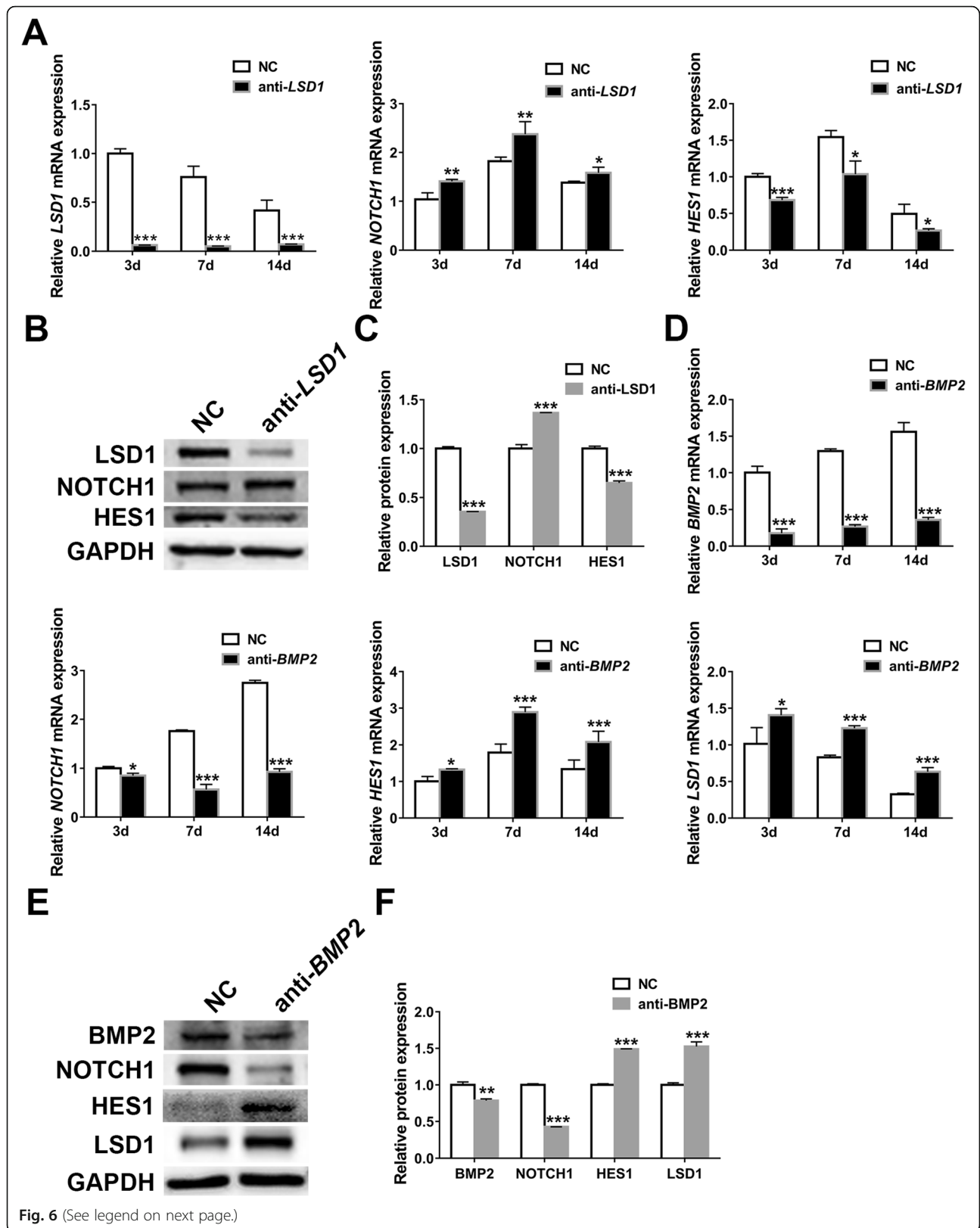
***NOTCH1* knockdown induces *LSD1* while inhibits *BMP2-SMADs* pathway**

Since our previous study has demonstrated that miR-137 upregulated *LSD1* while downregulated *BMP2* and *SMAD4* in hASCs [32], we further investigated the influences of *NOTCH1* knockdown on *LSD1* and *BMP2-SMADs* pathway. As predicted, the expression of *LSD1* significantly increased after knocking down *NOTCH1* while *BMP2*, *SMAD4*, and p-SMAD1/5 decreased apparently (Fig. 5). Therefore, we deduced that the osteogenic inhibition of *NOTCH1* knockdown is also dependent on the activation of *LSD1* and suppression of *BMP2-SMADs* pathway.

***LSD1* knockdown regulates *NOTCH1-HES1* pathway**

As above, we have affirmed that *NOTCH1* acted as a negative regulator in *LSD1* expression. But considering the





(See figure on previous page.)

Fig. 6 *LSD1* or *BMP2* knockdown influences *NOTCH1/LSD1/BMP2* signaling network. **a** Relative expression analyses of *LSD1*, *NOTCH1*, and *HES1* by qRT-PCR in transfected hASCs on 3 days, 7 days, and 14 days. **b, c** Western blotting (**b**) and band intensity analyses (**c**) of *LSD1*, *NOTCH1*, and *HES1* in transfected hASCs on 7 days. **d** Relative expression analyses of *BMP2*, *NOTCH1*, *HES1*, and *LSD1* by qRT-PCR in transfected hASCs on 3 days, 7 days, and 14 days. **e, f** Western blotting (**e**) and band intensity analyses (**f**) of *BMP2*, *NOTCH1*, *HES1*, and *LSD1* in transfected hASCs on 7 days. Data are shown as mean \pm SD of three independent experiments performed in triplicate. * $p < 0.05$, ** $p < 0.01$, *** $p < 0.001$ versus respective NC group

complex interplay of signaling molecules, we tried to clarify whether *LSD1* had feedback effects on *NOTCH1-HES1* pathway. Notably, we found that *LSD1* knockdown led to a higher level of *NOTCH1* while lowered the expression of *HES1* when compared with NC group (Fig. 6a–c), thus prompting a reciprocal negative relationship between *NOTCH1* and *LSD1*.

BMP2* knockdown inhibits *NOTCH1* while induces *HES1* and *LSD1

To gain further insights into the relationships between *NOTCH1*, *LSD1*, and *BMP2* signals, we then examined the expression of *NOTCH1*, *HES1*, and *LSD1* at mRNA and protein levels after knocking down *BMP2*. Importantly, the expression of *NOTCH1* dramatically decreased while *HES1* and *LSD1* increased with *BMP2* knockdown (Fig. 6d–f). Combining with the above results that *NOTCH1* knockdown inhibited *BMP2-SMADs* pathway, we verified a positive feedback loop between *NOTCH1* and *BMP2*. Furthermore, our previous study revealed that silencing of *LSD1* promoted the osteoblastic potential of hASCs by stimulating *BMP2-SMAD4* signaling pathway [32]. Here again, we observed upward

tendencies in the expression of *BMP2*, *SMAD4*, *RUNX2*, and *ALP* with *LSD1* knockdown (Additional file 4: Fig. S4). Therefore, a negative interplay between *LSD1* and *BMP2* was also confirmed by us.

Discussion

Dysfunction of miR-137 has been implicated in several cancer types such as glioblastoma [19], melanoma [20], multiple myeloma [21], non-small cell lung cancer [22], and endometrial cancer [23]. In addition, miR-137 has been found to play an essential role in neural development and maturation, with several studies displaying an association with cell proliferation and neurogenic differentiation [24–31]. However, little is known concerning its functions and regulatory mechanisms on the osteoblastic differentiation, especially in mesenchymal stem cells. Silencing of miR-137-3p is found to facilitate the osteogenesis of bone marrow-derived mesenchymal stem cells by targeting *RUNX2* [50]. Previously, we demonstrated that silencing of miR-137 promoted the osteoblastic activity in hASCs and revealed its modulation on the signaling network of *LSD1/BMP2/SMAD4* as part of the mechanisms [32]. Interestingly, our former research

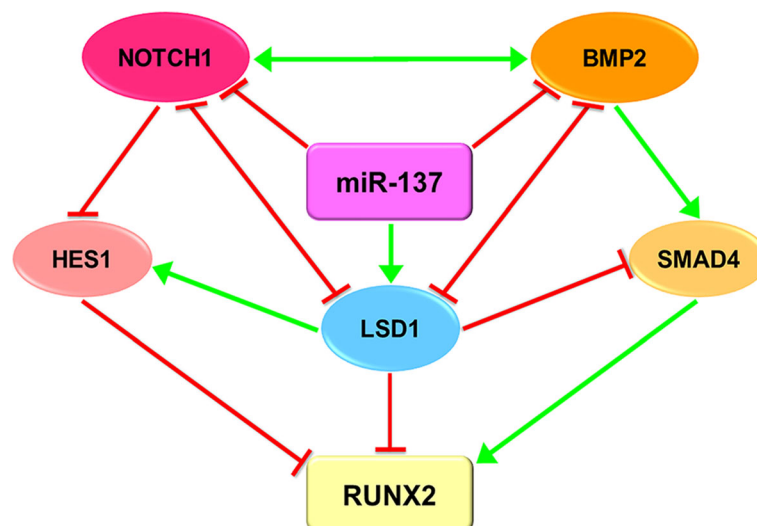


Fig. 7 A diagrammatic view of *NOTCH1/LSD1/BMP2* signaling network in miR-137-mediated differentiation of hASCs towards osteoblastic lineage. In this complex network model, miR-137 modulates *NOTCH1-HES1*, *LSD1*, and *BMP2-SMADs* pathways simultaneously. Depending on the positive feedback loop between *NOTCH1* and *BMP2*, as well as the negative reciprocal relationship between *LSD1* and *NOTCH1* or *BMP2*, the impacts of miR-137 on the above three signaling pathways are strengthened and the *NOTCH1/LSD1/BMP2* network regulates the osteogenesis of hASCs coordinately (red lines represent downregulation and green lines represent upregulation)

confirmed a positive role of miR-137 in *LSI1* expression, which was contrary to several studies reporting that miR-137 directly binds to *LSI1* [23, 26, 51, 52]. The contradicted outcomes might be associated with the various biological features of different cell types, and we deduced that there probably exist intermediary regulators working between miR-137 and *LSI1* during the osteogenesis of hASCs. Notably, this study identified that *NOTCH1* was a direct target of miR-137 in hASCs, and *NOTCH1-HES1* pathway was engaged in the crosstalk between *LSI1* and *BMP2-SMADs* pathway. In this way, *NOTCH1* signal mediated the control of miR-137 on *LSI1/BMP2/SMAD4* network. Moreover, the interrelations of the above signals were validated comprehensively and a *NOTCH1/LSI1/BMP2* co-regulatory network was established, further elucidating the epigenetic mechanisms of miR-137 during the process of hASCs differentiating into osteoblastic lineage.

After reconfirming the inhibitory impacts of miR-137 on the osteoblastic activity of hASCs both in vitro and in vivo, we demonstrated that miR-137 negatively regulated the expression of *NOTCH1* while positively regulated *HES1*. *NOTCH* signaling pathway influences tumorigenesis as well as embryonic development [53] because of its crucial role in cell fate determination, proliferation, differentiation, and apoptosis [54]. Though it is still debatable whether *NOTCH* signal serves as a positive or negative regulator in osteogenesis [55], our data displayed impaired osteogenic capacity of hASCs after knocking down *NOTCH1*. Most noteworthy, *NOTCH1* was validated as a direct target gene of miR-137 in hASCs, the same as in other cell lines [40–44]. *HES1* is known as a potential downstream gene of *NOTCH1* in many studies, but it is not affected in *NOTCH1* knockout mice while the expression of *HES5* and *HES-related repressor protein (HERP)1, -2, and -3* are greatly diminished [56–58]. As a transcriptional regulator in the *NOTCH* signaling pathway, *recombination signal binding protein (RBPJ)* gene disruption in homozygous mice exhibits reduced *HES5* expression, but not for *HES1* [56]. Given the various effects on *OCN*, *osteopontin*, and *RUNX2* [37, 38], *HES1* influences the osteogenesis inconsistently depending on the different cellular environments. This study exhibited enhanced osteogenic differentiation of hASCs with *HES1* knockdown. Moreover, *NOTCH1* knockdown upregulated *HES1*, indicating that *NOTCH1* acts as a negative regulator in the expression of *HES1*. To further identify whether *NOTCH1* mediated the osteogenic differentiation of hASCs modulated by miR-137, we applied *NOTCH1* inhibitor (tangeretin) in hASCs transfected with miR-137 knockdown lentiviruses and found that tangeretin reversed the impacts of miR-137 knockdown on osteogenesis and downstream genes expression, thus verifying

the vital role of *NOTCH1* in the osteogenic regulation of miR-137. Collectively, we brought insight into how the *NOTCH1-HES1* pathway was influenced and involved in the osteogenic modulation of miR-137.

LSI1 has been linked to the repression of *NOTCH1* pathway in various cell types [45, 59–63], though one study states that it functions as a corepressor when associated with *RBPJ*-repressor complex and as a *NOTCH1* coactivator upon *NOTCH* activation [64]. Nevertheless, few studies have reported the interplay between *NOTCH1* and *LSI1* during the osteogenesis of hASCs and whether this interaction contributes to the osteogenic control of miR-137 is still unknown. Coincident with the influences of miR-137 on *NOTCH1* and *LSI1*, we uncovered a negative interaction between *NOTCH1* and *LSI1* with separate knockdown of them. More intriguingly, despite inducing the expression of *NOTCH1*, *LSI1* knockdown repressed *HES1*. Thus, the opposite expression trends of *NOTCH1* and *HES1* caused by *LSI1* knockdown might reinforce the downregulation of *HES1* by *NOTCH1* alone. These results authenticated the crosstalk between *NOTCH1-HES1* pathway and *LSI1*, through which miR-137 regulates the osteogenic differentiation of hASCs.

BMP signal is a canonical pathway in skeleton and *BMP2-SMAD4* pathway has been shown to participate in the osteogenic regulation of miR-137 by us [32]. After knocking down *NOTCH1* or *BMP2* individually, we observed suppressed expression of *NOTCH1*, *BMP2*, and *SMADs* simultaneously, indicating a positive interrelationship between *NOTCH1* and *BMP2-SMADs* pathway. Besides, increased *HES1* expression with *BMP2* knockdown proved the negative effects of *NOTCH1* on *HES1* from another aspect. Considering our previous results that *LSI1* knockdown activated the *BMP2-SMAD4* pathway [32], in turn, we investigated the impacts of *BMP2* on *LSI1*. As expected, *LSI1* was significantly upregulated with *BMP2* knockdown. Thus, these findings suggested a negative feedback loop between *LSI1* and *BMP2-SMADs* pathway.

In conclusion, our results revealed that depending on the reciprocal negative regulation between *NOTCH1* and *LSI1*, *LSI1* and *BMP2*, as well as the synergistic function between *NOTCH1* and *BMP2*, miR-137 negatively regulates osteogenesis of hASCs through the *NOTCH1/LSI1/BMP2* co-regulatory signaling network (Fig. 7).

Conclusions

In summary, our study provided a relatively comprehensive rationale for the negative modulation of miR-137 during the hASC differentiation towards osteoblastic lineage and established a co-regulatory network of *NOTCH1/LSI1/BMP2* to elucidate the underlying

mechanisms, which is of substantial importance for potential targeted therapy of bone-related diseases.

Abbreviations

3' UTR: 3' untranslated region; ACPC: Auto-setting calcium phosphate cement; ALP: Alkaline phosphatase; ARS: Alizarin red S; *BMP*: Bone morphogenetic protein; GFP: Green fluorescent protein; hASCs: Human adipose-derived stem cells; HE: Hematoxylin and eosin; *HES1*: Hairy and enhancer of split 1; IHC: Immunohistochemical; LSD1: Lysine-specific histone demethylase 1; miRNA: MicroRNA; OCN: Osteocalcin; OM: Osteogenic medium; PM: Proliferation medium; qRT-PCR: Quantitative real-time polymerase chain reaction; RUNX2: Runt-related transcription factor 2; SMAD4: Mothers against decapentaplegic homolog 4; p-SMAD1/5: Phosphorylated SMAD1/5

Supplementary Information

The online version contains supplementary material available at <https://doi.org/10.1186/s13287-021-02495-3>.

Additional file 1: Figure S1. Efficiency determination of lentiviral transfection. a The structure diagram of packaged lentiviruses. b Microscopic images of transfected hASCs with GFP-tagged lentiviruses under the ordinary (left panel) and fluorescent light (right panel). Scale bar = 100 μ m. c Relative expression analysis of miR-137 by qRT-PCR in transfected hASCs on 3 d, 7 d and 14 d. Data are shown as mean \pm SD of three independent experiments performed in triplicate. * $p < 0.05$, ** $p < 0.01$, *** $p < 0.001$ versus respective NC group.

Additional file 2: Figure S2. MiR-137 reversely regulates hASC differentiation along osteoblastic lineage *in vitro*. a, b ALP staining (a) and quantification (b) of transfected hASCs after a 7-day culture in PM or OM (scale bar = 100 μ m). c, d ARS staining (c) and quantification (d) of transfected hASCs after a 14-day culture in PM or OM. e Relative expression analyses of *RUNX2*, *ALP* and *OCN* by qRT-PCR in transfected hASCs on 3 d, 7 d and 14 d. Data are shown as mean \pm SD of three independent experiments performed in triplicate. * $p < 0.05$, ** $p < 0.01$, *** $p < 0.001$ versus respective NC group.

Additional file 3: Figure S3. MiR-137 reversely regulates hASC differentiation along osteoblastic lineage *in vivo*. a Schema of the experimental design for *in vivo* study. $n = 6$ per group. b Representative soft X-ray photographs of the specimens which were subcutaneously harvested from the dorsal pockets of nude mice 8 weeks later. c Mean density analyses by the application of ImageJ software. Data are shown as mean \pm SD of six independent experiments. * $p < 0.05$, ** $p < 0.01$, *** $p < 0.001$ versus NC group. d Heterotopic bone formation was evaluated by histological stainings: HE, Masson trichrome staining (scale bar = 50 μ m), and IHC staining of OCN (scale bar = 20 μ m). Typical dark brown particles indicating OCN depositions in hASCs were marked with black arrows.

Additional file 4: Figure S4. *LSD1* knockdown activates *BMP2-SMAD4* pathway and osteogenesis-associated genes expression. a Relative expression analyses of *BMP2*, *SMAD4*, *RUNX2* and *ALP* by qRT-PCR in transfected hASCs on 3 d, 7 d and 14 d. b, c Western blotting (b) and band intensity analyses (c) of LSD1, BMP2, SMAD4 and RUNX2 in transfected hASCs on 7 d. Data are shown as mean \pm SD of three independent experiments performed in triplicate. * $p < 0.05$, ** $p < 0.01$, *** $p < 0.001$ versus respective NC group.

Additional file 5: Table S1. Sequences for lentiviral vectors.

Additional file 6: Table S2. Sequences of the primers for qRT-PCR.

Additional file 7: Table S3. Key resources table.

Acknowledgements

Not applicable.

Authors' contributions

CF conceived the project, provided financial supports, and wrote the manuscript. XM performed the main experiments, analyzed data and prepared figures. YW, LL, YZ, and HL helped with the animal work. YL assisted with the data analysis and offered insightful ideas.

Funding

This study was financially granted by grants from the National Natural Science Foundation of China (No. 81700937 and No. 81930026), and Beijing Natural Science Foundation (No. L182006).

Availability of data and materials

The datasets used and analyzed during the current study are available from the corresponding author on reasonable request.

Declarations

Ethics approval and consent to participate

This study was approved by the Institutional Animal Care and Use Committee of the Peking University Health Science Center (Approval No. LA2019019).

Consent for publication

Not applicable.

Competing interests

The authors declare that they have no competing interests.

Author details

¹Department of General Dentistry II, Peking University School and Hospital of Stomatology, Beijing, China. ²National Center of Stomatology, Beijing, China. ³National Clinical Research Center for Oral Diseases, Beijing, China. ⁴National Engineering Laboratory for Digital and Material Technology of Stomatology, Beijing, China. ⁵Research Center of Engineering and Technology for Computerized Dentistry Ministry of Health, Beijing, China. ⁶NMPA Key Laboratory for Dental Materials, Beijing, China. ⁷Department of Prosthodontics, Peking University School and Hospital of Stomatology, Beijing, China. ⁸Department of Prosthodontics, Beijing Stomatological Hospital Capital Medical University, Beijing, China. ⁹Central Laboratory, Peking University School and Hospital of Stomatology, Beijing, China.

Received: 31 August 2020 Accepted: 5 July 2021

Published online: 22 July 2021

References

- Deng Y, Zhou H, Zou D, Xie Q, Bi X, Gu P, et al. The role of miR-31-modified adipose tissue-derived stem cells in repairing rat critical-sized calvarial defects. *Biomaterials*. 2013;34(28):6717–28. <https://doi.org/10.1016/j.biomaterials.2013.05.042>.
- Hao W, Liu H, Zhou L, Sun Y, Su H, Ni J, et al. MiR-145 regulates osteogenic differentiation of human adipose-derived mesenchymal stem cells through targeting FoxO1. *Exp Biol Med* (Maywood). 2018;243(4):386–93. <https://doi.org/10.1177/1535370217746611>.
- Lin CY, Chang YH, Li KC, Lu CH, Sung LY, Yeh CL, et al. The use of ASCs engineered to express BMP2 or TGF- β 3 within scaffold constructs to promote calvarial bone repair. *Biomaterials*. 2013;34(37):9401–12. <https://doi.org/10.1016/j.biomaterials.2013.08.051>.
- Ullah I, Subbarao RB, Rho GJ. Human mesenchymal stem cells-current trends and future prospective. *Biosci Rep*. 2015;35(2):e00191. <https://doi.org/10.1042/BSR20150025>.
- Zhang WB, Zhong WJ, Wang L. A signal-amplification circuit between miR-218 and Wnt/ β -catenin signal promotes human adipose tissue-derived stem cells osteogenic differentiation. *Bone*. 2014;58:59–66. <https://doi.org/10.1016/j.bone.2013.09.015>.
- Becker M, Potapenko T, Niklaus A, Bieback K, Ho AD, Müller AM. Polycomb protein BMI1 regulates osteogenic differentiation of human adipose tissue-derived mesenchymal stem cells downstream of GSK3. *Stem Cells Dev*. 2016;25(12):922–33. <https://doi.org/10.1089/scd.2015.0277>.
- Quarto N, Senarath-Yapa K, Renda A, Longaker MT. TWIST1 silencing enhances *in vitro* and *in vivo* osteogenic differentiation of human adipose-derived stem cells by triggering activation of BMP-ERK/FGF signaling and TAZ upregulation. *Stem Cells*. 2015;33(3):833–47. <https://doi.org/10.1002/stem.1907>.
- Vanhatupa S, Ojansivu M, Autio R, Juntunen M, Miettinen S. Bone morphogenetic protein-2 induces donor-dependent osteogenic and adipogenic differentiation in human adipose stem cells. *Stem Cells Transl Med*. 2015;4(12):1391–402. <https://doi.org/10.5966/sctm.2015-0042>.

9. Zhang Z, Ma Y, Guo S, He Y, Bai G, Zhang W. Low-intensity pulsed ultrasound stimulation facilitates *in vitro* osteogenic differentiation of human adipose-derived stem cells via up-regulation of heat shock protein (HSP)70, HSP90, and bone morphogenetic protein (BMP) signaling pathway. *Biosci Rep*. 2018;38(3):BSR20180087. <https://doi.org/10.1042/BSR20180087>.
10. Fan C, Jia L, Zheng Y, Jin C, Liu Y, Liu H, et al. MiR-34a promotes osteogenic differentiation of human adipose-derived stem cells via the RBP2/NOTCH1/CYCLIN D1 coregulatory network. *Stem Cell Reports*. 2016;7(2):236–48. <https://doi.org/10.1016/j.stemcr.2016.06.010>.
11. Lough DM, Chambers C, Germann G, Bueno R, Reichensperger J, Swanson E, et al. Regulation of ADSC osteoinductive potential using Notch pathway inhibition and gene rescue: a potential on/off switch for clinical applications in bone formation and reconstructive efforts. *Plast Reconstr Surg*. 2016; 138(4):642e–52e.
12. Aimaity A, Maimaitiyiming A, Boyong X, Aji K, Li C, Cui L. Low-dose strontium stimulates osteogenesis but high-dose doses cause apoptosis in human adipose-derived stem cells via regulation of the ERK1/2 signaling pathway. *Stem Cell Res Ther*. 2017;8(1):282. <https://doi.org/10.1186/s13287-017-0726-8>.
13. Zhang M, Zhang P, Liu Y, Lv L, Zhang X, Liu H, et al. RSP03-LGR4 regulates osteogenic differentiation of human adipose-derived stem cells via ERK/FGF signalling. *Sci Rep*. 2017;7(1):42841. <https://doi.org/10.1038/srep42841>.
14. Ambros V. The functions of animal microRNAs. *Nature*. 2004;431(7006):350–5. <https://doi.org/10.1038/nature02871>.
15. Chen S, Zheng Y, Zhang S, Jia L, Zhou Y. Promotion effects of miR-375 on the osteogenic differentiation of human adipose-derived mesenchymal stem cells. *Stem Cell Reports*. 2017;8(3):773–86. <https://doi.org/10.1016/j.stemcr.2017.01.028>.
16. Kim YJ, Bae SW, Yu SS, Bae YC, Jung JS. MiR-196a regulates proliferation and osteogenic differentiation in mesenchymal stem cells derived from human adipose tissue. *J Bone Miner Res*. 2009;24(5):816–25. <https://doi.org/10.1359/jbmr.081230>.
17. Liao YH, Chang YH, Sung LY, Li KC, Yeh CL, Yen TC, et al. Osteogenic differentiation of adipose-derived stem cells and calvarial defect repair using baculovirus-mediated co-expression of BMP-2 and miR-148b. *Biomaterials*. 2014;35(18):4901–10. <https://doi.org/10.1016/j.biomaterials.2014.02.055>.
18. Zeng Y, Qu X, Li H, Huang S, Wang S, Xu Q, et al. MicroRNA-100 regulates osteogenic differentiation of human adipose-derived mesenchymal stem cells by targeting BMPR2. *FEBS Lett*. 2012;586(16):2375–81. <https://doi.org/10.1016/j.febslet.2012.05.049>.
19. Li D, Shan W, Fang Y, Wang P, Li J. MiR-137 acts as a tumor suppressor via inhibiting CXCL12 in human glioblastoma. *Oncotarget*. 2017;8(60):101262–70. <https://doi.org/10.18632/oncotarget.20589>.
20. Luo M, Wu L, Zhang K, Wang H, Zhang T, Gutierrez L, et al. MiR-137 regulates ferroptosis by targeting glutamine transporter SLC1A5 in melanoma. *Cell Death Differ*. 2018;25(8):1457–72. <https://doi.org/10.1038/s41418-017-0053-8>.
21. Qin Y, Zhang S, Deng S, An G, Qin X, Li F, et al. Epigenetic silencing of miR-137 induces drug resistance and chromosomal instability by targeting AURKA in multiple myeloma. *Leukemia*. 2017;31(5):1123–35. <https://doi.org/10.1038/leu.2016.325>.
22. Liu X, Chen L, Tian XD, Zhang T. MiR-137 and its target TGFA modulate cell growth and tumorigenesis of non-small cell lung cancer. *Eur Rev Med Pharmacol Sci*. 2017;21(3):511–7.
23. Zhang W, Chen JH, Shan T, Aguilar-Barrantes I, Wang LS, Huang TH, et al. MiR-137 is a tumor suppressor in endometrial cancer and is repressed by DNA hypermethylation. *Lab Invest*. 2018;98(11):1397–407. <https://doi.org/10.1038/s41374-018-0092-x>.
24. Jiang K, Ren C, Nair VD. MicroRNA-137 represses Klf4 and Tbx3 during differentiation of mouse embryonic stem cells. *Stem Cell Res*. 2013;11(3): 1299–313. <https://doi.org/10.1016/j.scr.2013.09.001>.
25. Silber J, Lim DA, Petritsch C, Persson AI, Maunake AK, Yu M, et al. MiR-124 and miR-137 inhibit proliferation of glioblastoma multiforme cells and induce differentiation of brain tumor stem cells. *BMC Med*. 2008;6(1):14. <https://doi.org/10.1186/1741-7015-6-14>.
26. Sun GQ, Ye P, Murai K, Lang MF, Li S, Zhang H, et al. MiR-137 forms a regulatory loop with nuclear receptor TLX and LSD1 in neural stem cells. *Nat Commun*. 2011;2(1):529. <https://doi.org/10.1038/ncomms1532>.
27. Szulwach KE, Li X, Smrt RD, Li Y, Luo Y, Lin L, et al. Cross talk between microRNA and epigenetic regulation in adult neurogenesis. *J Cell Biol*. 2010; 189(1):127–41. <https://doi.org/10.1083/jcb.200908151>.
28. Tarantino C, Paoletta G, Cozzuto L, Minopoli G, Pastore L, Parisi S, et al. MiRNA 34a, 100, and 137 modulate differentiation of mouse embryonic stem cells. *FASEB J*. 2010;24(9):3255–63. <https://doi.org/10.1096/fj.09-152207>.
29. Crowley JJ, Collins AL, Lee RJ, Nonneman RJ, Farrell MS, Ancalade N, et al. Disruption of the microRNA 137 primary transcript results in early embryonic lethality in mice. *Biol Psychiatry*. 2015;77(2):e5–7. <https://doi.org/10.1016/j.biopsych.2014.05.022>.
30. Hollins SL, Goldie BJ, Carroll AP, Mason EA, Walker FR, Eyles DW, et al. Ontogeny of small RNA in the regulation of mammalian brain development. *BMC Genomics*. 2014;15(1):777. <https://doi.org/10.1186/1471-2164-15-777>.
31. Smrt RD, Szulwach KE, Pfeiffer RL, Li X, Guo W, Pathania M, et al. MicroRNA miR-137 regulates neuronal maturation by targeting ubiquitin ligase mind bomb-1. *Stem Cells*. 2010;28(6):1060–70. <https://doi.org/10.1002/stem.431>.
32. Ma X, Fan C, Wang Y, Du Y, Zhu Y, Liu H, et al. MiR-137 knockdown promotes the osteogenic differentiation of human adipose-derived stem cells via the LSD1/BMP2/SMAD4 signaling network. *J Cell Physiol*. 2020; 235(2):909–19. <https://doi.org/10.1002/jcp.29006>.
33. Canalis E, Adams DJ, Boskey A, Parker K, Kranz L, Zanotti S. Notch signaling in osteocytes differentially regulates cancellous and cortical bone remodeling. *J Biol Chem*. 2013;288(35):25614–25. <https://doi.org/10.1074/jbc.M113.470492>.
34. Engin F, Yao Z, Yang T, Zhou G, Bertin T, Jiang MM, et al. Dimorphic effects of Notch signaling in bone homeostasis. *Nat Med*. 2008;14(3):299–305. <https://doi.org/10.1038/nm1712>.
35. Zanotti S, Canalis E. Notch signaling and the skeleton. *Endocr Rev*. 2016; 37(3):223–53. <https://doi.org/10.1210/er.2016-1002>.
36. Jarriault S, Brou C, Logeat F, Schroeter EH, Kopan R, Israel A. Signalling downstream of activated mammalian Notch. *Nature*. 1995;377(6547):355–8. <https://doi.org/10.1038/377355a0>.
37. Shen Q, Christakos S. The vitamin D receptor, Runx2, and the Notch signaling pathway cooperate in the transcriptional regulation of osteopontin. *J Biol Chem*. 2005;280(49):40589–98. <https://doi.org/10.1074/jbc.M504166200>.
38. Zhang Y, Lian JB, Stein JL, van Wijnen AJ, Stein GS. The Notch-responsive transcription factor Hes-1 attenuates osteocalcin promoter activity in osteoblastic cells. *J Cell Biochem*. 2009;108(3):651–9. <https://doi.org/10.1002/jcb.22299>.
39. Zanotti S, Smerdel-Ramoya A, Canalis E. HES1 (hairly and enhancer of split 1) is a determinant of bone mass. *J Biol Chem*. 2011;286(4):2648–57. <https://doi.org/10.1074/jbc.M110.183038>.
40. Han F, Wang S, Chang Y, Li C, Yang J, Han Z, et al. Triptolide prevents extracellular matrix accumulation in experimental diabetic kidney disease by targeting microRNA-137/Notch1 pathway. *J Cell Physiol*. 2018;233(3):2225–37. <https://doi.org/10.1002/jcp.26092>.
41. Li H, Zhu Z, Liu J, Wang J, Qu C. MicroRNA-137 regulates hypoxia-induced retinal ganglion cell apoptosis through Notch1. *Int J Mol Med*. 2018;41(3): 1774–82. <https://doi.org/10.3892/ijmm.2017.3319>.
42. Shi F, Dong Z, Li H, Liu X, Liu H, Dong R. MicroRNA-137 protects neurons against ischemia/reperfusion injury through regulation of the Notch signaling pathway. *Exp Cell Res*. 2017;352(1):1–8. <https://doi.org/10.1016/j.yexcr.2017.01.015>.
43. Wang X, Zhang G, Cheng Z, Dai L, Jia L, Jing X, et al. Knockdown of lncRNA-XIST suppresses proliferation and TGF-β1-induced EMT in NSCLC through the Notch-1 pathway by regulation of miR-137. *Genet Test Mol Biomarkers*. 2018;22(6):333–42. <https://doi.org/10.1089/gtmb.2018.0026>.
44. Zeng JS, Zhang ZD, Pei L, Bai ZZ, Yang Y, Yang H, et al. CBX4 exhibits oncogenic activities in breast cancer via Notch1 signaling. *Int J Biochem Cell Biol*. 2018;95:1–8. <https://doi.org/10.1016/j.biocel.2017.12.006>.
45. Augert A, Eastwood E, Ibrahim AH, Wu N, Grunblatt E, Basom R, et al. Targeting NOTCH activation in small cell lung cancer through LSD1 inhibition. *Sci Signal*. 2019;12(567):eaau2922.
46. Viale-Bouroncle S, Gosau M, Morszczek C. NOTCH1 signaling regulates the BMP2/DLX-3 directed osteogenic differentiation of dental follicle cells. *Biochem Biophys Res Commun*. 2014;443(2):500–4. <https://doi.org/10.1016/j.bbrc.2013.11.120>.
47. Wang D, Zeng Q, Song R, Ao L, Fullerton DA, Meng X. Ligation of ICAM-1 on human aortic valve interstitial cells induces the osteogenic response: a critical role of the Notch1-NF-κB pathway in BMP-2 expression. *Biochim Biophys Acta*. 2014;1843(11):2744–53. <https://doi.org/10.1016/j.bbamcr.2014.07.017>.

48. Sun J, Ermann J, Niu N, Yan G, Yang Y, Shi Y, et al. Histone demethylase LSD1 regulates bone mass by controlling WNT7B and BMP2 signaling in osteoblasts. *Bone Res.* 2018;6(1):14. <https://doi.org/10.1038/s41413-018-0015-x>.
49. Yang C, Wang W, Liang JX, Li G, Vellaisamy K, Wong CY, et al. A rhodium (III)-based inhibitor of lysine-specific histone demethylase 1 as an epigenetic modulator in prostate cancer cells. *J Med Chem.* 2017;60(6):2597–603. <https://doi.org/10.1021/acs.jmedchem.7b00133>.
50. Kong L, Zuo R, Wang M, Wang W, Xu J, Chai Y, et al. Silencing microRNA-137-3p, which targets RUNX2 and CXCL12 prevents steroid-induced osteonecrosis of the femoral head by facilitating osteogenesis and angiogenesis. *Int J Biol Sci.* 2020;16(4):655–70. <https://doi.org/10.7150/ijbs.38713>.
51. Althoff K, Beckers A, Odersky A, Mestdagh P, Köster J, Bray IM, et al. MiR-137 functions as a tumor suppressor in neuroblastoma by downregulating KDM1A. *Int J Cancer.* 2013;133(5):1064–73. <https://doi.org/10.1002/ijc.28091>.
52. Chen L, Wang X, Huang W, Ying T, Chen M, Cao J, et al. MicroRNA-137 and its downstream target LSD1 inversely regulate anesthetics-induced neurotoxicity in dorsal root ganglion neurons. *Brain Res Bull.* 2017;135:1–7. <https://doi.org/10.1016/j.brainresbull.2017.09.004>.
53. Hartenstein AY, Rugendorff A, Tepass U, Hartenstein V. The function of the neurogenic genes during epithelial development in the drosophila embryo. *Development.* 1992;116(4):1203–20. <https://doi.org/10.1242/dev.116.4.1203>.
54. Miele L, Osborne B. Arbiter of differentiation and death: Notch signaling meets apoptosis. *J Cell Physiol.* 1999;181(3):393–409. [https://doi.org/10.1002/\(SICI\)1097-4652\(199912\)181:3<393:AID-JCP3>3.0.CO;2-6](https://doi.org/10.1002/(SICI)1097-4652(199912)181:3<393:AID-JCP3>3.0.CO;2-6).
55. Ongaro A, Pellati A, Bagheri L, Rizzo P, Caliceti C, Massari L, et al. Characterization of Notch signaling during osteogenic differentiation in human osteosarcoma cell line MG63. *J Cell Physiol.* 2016;231(12):2652–63. <https://doi.org/10.1002/jcp.25366>.
56. de la Pompa JL, Wakeham A, Correia KM, Samper E, Brown S, Aguilera RJ, et al. Conservation of the Notch signalling pathway in mammalian neurogenesis. *Development.* 1997;124(6):1139–48. <https://doi.org/10.1242/dev.124.6.1139>.
57. Leimeister C, Dale K, Fischer A, Klamt B, Hrabec de Angelis M, Radtke F, et al. Oscillating expression of c-Hey2 in the presomitic mesoderm suggests that the segmentation clock may use combinatorial signaling through multiple interacting bHLH factors. *Dev Biol.* 2000;227(1):91–103. <https://doi.org/10.1006/dbio.2000.9884>.
58. Leimeister C, Schumacher N, Steidl C, Gessler M. Analysis of Heyl expression in wild-type and Notch pathway mutant mouse embryos. *Mech Dev.* 2000; 98(1–2):175–8. [https://doi.org/10.1016/S0925-4773\(00\)00459-7](https://doi.org/10.1016/S0925-4773(00)00459-7).
59. Di Stefano L, Walker JA, Burgio G, Corona DF, Mulligan P, Näär AM, et al. Functional antagonism between histone H3K4 demethylases in vivo. *Genes Dev.* 2011;25(1):17–28. <https://doi.org/10.1101/gad.1983711>.
60. Han X, Ranganathan P, Tzimas C, Weaver KL, Jin K, Astudillo L, et al. Notch represses transcription by PRC2 recruitment to the ternary complex. *Mol Cancer Res.* 2017; 15(9):1173–83. <https://doi.org/10.1158/1541-7786.MCR-17-0241>.
61. Lopez CI, Saud KE, Aguilar R, Berndt FA, Cánovas J, Montecino M, et al. The chromatin modifying complex CoREST/LSD1 negatively regulates notch pathway during cerebral cortex development. *Dev Neurobiol.* 2016;76(12): 1360–73. <https://doi.org/10.1002/dneu.22397>.
62. Mulligan P, Yang F, Di Stefano L, Ji JY, Ouyang J, Nishikawa JL, et al. A SIRT1-LSD1 corepressor complex regulates Notch target gene expression and development. *Mol Cell.* 2011;42(5):689–99. <https://doi.org/10.1016/j.molcel.2011.04.020>.
63. Xu T, Park SS, Giaimo BD, Hall D, Ferrante F, Ho DM, et al. RBPJ/CBF1 interacts with L3MBTL3/MBT1 to promote repression of Notch signaling via histone demethylase KDM1A/LSD1. *EMBO J.* 2017;36(21):3232–49. <https://doi.org/10.15252/embj.201796525>.
64. Yatim A, Benne C, Sobhian B, Laurent-Chabalier S, Deas O, Judde JG, et al. NOTCH1 nuclear interactome reveals key regulators of its transcriptional activity and oncogenic function. *Mol Cell.* 2012;48(3):445–58. <https://doi.org/10.1016/j.molcel.2012.08.022>.

Publisher's Note

Springer Nature remains neutral with regard to jurisdictional claims in published maps and institutional affiliations.

Ready to submit your research? Choose BMC and benefit from:

- fast, convenient online submission
- thorough peer review by experienced researchers in your field
- rapid publication on acceptance
- support for research data, including large and complex data types
- gold Open Access which fosters wider collaboration and increased citations
- maximum visibility for your research: over 100M website views per year

At BMC, research is always in progress.

Learn more biomedcentral.com/submissions

